Towards Identification of a Reliable Framework to Predict the Thermal Field in Turbulent Wall-Bounded Shear Flows

Ziefuss M.[1], Karimi N.[2] and Mehdizadeh A.[1]*

[1] School of Computing and Engineering, Civil and Mechanical Engineering Department,
University of Missouri-Kansas City, Kansas City, MO 64110, United States

[2] School of Engineering and Materials Science,
Queen Mary University of London, London E1 4NS, United Kingdom

* Corresponding author: mehdizadeha@umkc.edu

Abstract
Heat transfer modeling plays an integral role in design and optimization of traditional, as well as modern emerging thermal-fluid systems. However, mostly available models, known as eddy diffusivity models, face challenges in prediction of second order statistics such as heat fluxes in homogeneous directions and temperature variance. Additionally, these models are developed targeting fluids with Prandtl (Pr) number around unity and thus, having difficulty to capture thermal fields of working fluids with Pr numbers significantly different than unity at an acceptable level of accuracy. In an attempt to take first step to address the existing shortcomings, this investigation aims to identify a reliable framework to predict the turbulent thermal field of fluids with different Pr numbers (0.025, 0.71 and 10) in wall-bounded shear flows. Towards this, most advanced models, i.e. implicit and explicit algebraic turbulent heat flux models that try to incorporate the anisotropic nature of the turbulent heat flux, have been applied to a turbulent attached boundary layer of various working fluids with significantly different Pr numbers. It turns out that the explicit framework based on the representation theory is potentially capable of dealing with complex turbulent thermal fields and to address shortcomings of currently available models. Moreover, it has been shown that thermal time scale plays an integral role to accurately predict thermal field of fluids with Pr numbers significantly different than unity, as well as high order statistical quantities (e.g. temperature variance) of fluids with Pr numbers around unity.

	Name
$b_{ij} = \overline{u_i u_j}/2k - 1/3\delta_{ij}$	Reynolds stress anisotropy tensor
c_p	specific heat capacity at constant pressure
k	turbulent kinetic energy
p	pressure fluctuations
u_i	velocity fluctuations
$\overline{u_i u_j}$	Reynolds stress tensor
Pr	Prandtl
$\mathcal{R} = \tau_\theta/\tau_m$	thermal to mechanical time scale ratio
Re	Reynolds number
$Re_\tau = U_\tau \delta/\nu$	turbulent Reynolds number
S_T	source terms in temperature equation
T	mean temperature
$T_\tau = q_w/\rho c_p U_\tau$	friction temperature
U_i	mean velocity
$U_\tau = Re_\tau \nu/\delta$	friction velocity
$\alpha = \lambda/\rho c_p$	thermal diffusivity
δ	channel half height
δ_{ij}	Kronecker delta
ε	dissipation of kinetic energy
ε_θ	dissipation of the temperature variance
$\overline{\theta^2}$	temperature variance
λ	thermal conductivity
ν	kinematic viscosity
ν_t	turbulent kinematic viscosity
θ	temperature fluctuations
$\overline{\theta u_i}$	turbulent heat flux
ρ	density
$\tau_m = k/\varepsilon$	mechanical time scale
$\tau_\theta = \overline{\theta^2}/2\varepsilon_\theta$	thermal time scale
$\tau = \sqrt{\tau_m \tau_\theta}$	mixed time scale
$\overline{(\,)}$	mean value

1 Introduction

The passive transport of heat in a turbulent environment plays an integral role in development and optimization in various advanced and emerging systems. These include cooling systems for nuclear power plants, where liquid metal is used as coolant [28, 4], boiler systems for biomass combustion [19], and heat exchange devices in the petroleum/petrochemical industry [32], to name only a few. The design and optimization of such systems rely heavily on computational modeling and simulation as experimental investigations are either not possible or prohibitively expensive [35].

Development and optimization of such systems require insight into complex dynamics of heat and mass transfer inside the system, which necessitates the application of reliable models. Furthermore, the above mentioned applications impose an additional challenge for models in predicting the heat transport at an acceptable level of accuracy when the Prandtl (denoted as Pr) number of the working fluid is significantly different than unity [8, 3, 42], i.e. ranges from Pr << 1 for liquid metal to a few thousands for crude oils. Thus, understanding and correct modeling of heat transport have introduced a major challenge in the past decades [7]. One of the underlying challenges is the strong dependency of the thermal field (temperature) on the flow field, which often is highly turbulent. As a direct consequence, an appropriate model for the momentum transport is an indispensable necessity and therefore, the main focus of modeling in the past few decades has been placed on turbulent flow field modeling [36]. The intuitive assumption is that a better prediction of momentum quantities leads to a better prediction of thermal quantities. This has led to the formulation of the first order models for turbulent heat fluxes, i.e. the eddy diffusivity approach based on the Reynolds Analogy. While this approach is a drastic simplification of the physical mechanisms, it has been applied successfully to predict first order statistics such as mean temperature in a large number of industrial applications using Computational Fluid Dynamics (CFD) technique. It is worth noting that these applications mostly deal with working fluids with Pr number around unity [2]. It was shown in [41, 42, 8] that the eddy diffusivity approach suffers from serious shortcomings when applied to predict second order statistics or thermal field of fluids with Pr number different than unity. Further, due to the mathematical formulation of the eddy diffusivity models—the heat flux is proportional to the mean temperature gradient [18]—a non-existing temperature gradient leads to a non-existing heat flux, which leads to

inaccurate prediction of turbulent heat fluxes in homogeneous direction in turbulent shear flows [42].

In order to address the shortcomings of the eddy diffusivity models, several approaches with different levels of complexity have been proposed based on the concept of cross-streamwise mixing, which is known to be the major underlying mechanism for both momentum and heat transfer [36]. These include, the generalized gradient diffusion hypothesis (GGDH), which includes time scales for the momentum or temperature field [5, 11], and algebraic heat flux models (AFMs), which introduce additional correlations to predict the heat flux [25, 21, 18, 40, 26]. However, these approaches have never been extensively investigated and there is only limited information on prediction capabilities of these methods in the literature [30, 8]. Nevertheless, it should be noted that algebraic heat flux models may offer promising potential to overcome shortcomings of the classical methods, based on limited information available in the literature [8, 40, 15]. Therefore, this study centers these models and aims to provide a comprehensive assessment of these methods when applied to a fully attached turbulent boundary layer using different working fluids.

There are two major variants of the AFMs distinguished by two fundamental different approaches: implicit and explicit models. The former is a result of truncating the exact heat flux equation [15, 10], while the latter is derived based on the representation theorem [40, 26]. There are few recent efforts on applications of implicit methods to predict thermal behavior of low Pr number fluids in turbulent wall bounded channel flow [36, 34], which will be discussed in section 2.3.3. Although some improvements were achieved compared to the classical methods, these studies do not provide some relevant statistical quantities such as the heat fluxes and dissipation of temperature variance. Additionally, these studies mainly target fluids with Pr numbers less than unity, i.e. the implicit models were calibrated/tuned for low Pr number fluids, which limits the application of the models.

In contrast, there is only one study that uses the explicit model to predict the thermal field in a turbulent channel flow [26]. This study shows clear improvements as compared to the classical approach (eddy diffusivity). However, detailed results are only presented for a turbulent rotating channel flow with main emphasis on first order statistics.

The current study presents a comprehensive assessment of predictive capabilities of the most recent versions of implicit and explicit turbulent heat flux models for first and second order statistics, when applied to 3D wall-bounded shear flow using different working fluids.

Additionally, the assessment includes sensitivity analysis with respect to the turbulence model used to describe the flow field.

Moreover, both implicit and explicit models use only mechanical time scale in their formulations, as will be discussed in the following sections. As a result of this, relevance and effects of thermal time scale in prediction capability of heat flux models remains unclear. This investigation aims to study the effects of thermal time scale on the predictive capabilities of both models. Therefore, the existing mechanical time scale is modified by including the thermal time scale in both models (as shown in section 2.3) and results obtained by both original and modified models will be assessed and analyzed. However, it should be noted that the goal here is only to study model sensitivity to the inclusion of thermal time scale and therefore, no additional model calibrations/tuning have been performed after inclusion of the thermal time scale into the model.

The paper is organized as follows: in section 2, the governing equations including employed turbulence and heat flux models will be presented and discussed. In section 3, an overview of test cases and the numerical approach is provided. Results obtained from simulations are presented and discussed in section 4. The paper concludes with a summary and conclusion in section 5.

2 Governing Equations and Model Description

Two different turbulence models, including Launder-Sharma's $k-\varepsilon$ model [22] and Lien-Abe's $k-\varepsilon$ model, will be used. The major difference between these models is that Launder-Sharma's model is a linear eddy viscosity model, while Lien-Abe's is a non-linear eddy viscosity model. This model is based on Lien's $k-\varepsilon$ model [23], modified with the non-linear term proposed by Abe [1]. As it will be shown and discussed later, the non-linear model is capable of predicting the Reynolds Stress tensor with a remarkably higher accuracy compared to the linear model, which should lead to more accurate predictions of thermal quantities.

2.1 Turbulence Models

2.1.1 Launder and Sharma's $k-\varepsilon$ model

The Launder-Sharma $k-\varepsilon$ [22] model is one of the most commonly used linear models. Henceforth, this model **will be denoted as *LS***. It employs two transport equations, one for turbulent kinetic energy k, and one for the dissipation rate ε. The model equations read:

$$\frac{Dk}{Dt} = \frac{\partial}{\partial x_i}\left[\left(\nu + \frac{\nu_t}{\sigma_k}\right)\frac{\partial k}{\partial x_i}\right] + P_k - \varepsilon, \tag{1}$$

$$\frac{D\tilde{\varepsilon}}{Dt} = \frac{\partial}{\partial x_i}\left[\left(\nu + \frac{\nu_t}{\sigma_\varepsilon}\right)\frac{\partial \tilde{\varepsilon}}{\partial x_i}\right] + C_1 P_k \frac{\tilde{\varepsilon}}{k} - C_2 f_2 \frac{\tilde{\varepsilon}^2}{k} + E. \tag{2}$$

$$\text{Where} \quad P_k = -\overline{u_i u_j}\frac{\partial U_i}{\partial x_j}, \quad \nu_t = C_\mu f_\mu \frac{k^2}{\tilde{\varepsilon}} \quad \text{and} \quad -\overline{u_i u_j} = b_{ij} - \frac{2}{3}\delta_{ij}k. \tag{3}$$

Here, b_{ij} is the Reynolds stress anisotropy tensor and since this is a linear model, b_{ij} holds only a linear term (denoted as ${}^l b_{ij}$):

$$b_{ij} = {}^l b_{ij} = S_{ij} = \nu_t\left(\frac{\partial U_i}{\partial x_j} + \frac{\partial U_j}{\partial x_i}\right). \tag{4}$$

Further details on model constants and functions, i.e. $C_1, C_2, C_\mu, \sigma_k, \sigma_\varepsilon, f_2, f_\mu, \tilde{\varepsilon}, E$, are provided in [22].

2.1.2 Lien-Abe $k-\varepsilon$ model

As previously mentioned, the Lien-Abe model is based on the linear part of the $k-\varepsilon$ model proposed in [23] and employs the non-linear term introduced by Abe et. al [1]. This model **will be denoted as *LA*** in the current study, and below is a summary of the model equations:

$$\frac{Dk}{Dt} = \frac{\partial}{\partial x_i}\left[\left(\nu + \frac{\nu_t}{\sigma_k}\right)\frac{\partial k}{\partial x_i}\right] + P_k - \varepsilon, \tag{5}$$

$$\frac{D\varepsilon}{Dt} = \frac{\partial}{\partial x_i}\left[\left(\nu + \frac{\nu_t}{\sigma_\varepsilon}\right)\frac{\partial \varepsilon}{\partial x_i}\right] + C_{\varepsilon 1} P_k \frac{\varepsilon}{k} - C_{\varepsilon 2} f_2 \frac{\varepsilon^2}{k} + E(f_2), \tag{6}$$

where b_{ij} includes two further non-linear terms ($^{2}b_{ij}$ and $^{s}b_{ij}$), in addition to the linear term ($^{l}b_{ij}$) :

$$b_{ij} = {}^{l}b_{ij} + {}^{2}b_{ij} + {}^{s}b_{ij}. \tag{7}$$

These two additional terms are rather complex and further details are provided in [1] while details on model constants for the $k-\varepsilon$ equations and functions,i.e. $A_E, C_{\varepsilon 1}, C_{\varepsilon 2}, C_\mu, \kappa, y^*, \sigma_k, \sigma_\varepsilon, f_2, E(f_2), l_e$, are provided in [23] and [39].

2.2 Internal Energy Equation

The Reynolds-averaged internal energy equation reads as [10]:

$$\rho c_p \frac{DT}{Dt} = S_T + \frac{\partial}{\partial x_i}\left[\left(\lambda \frac{\partial T}{\partial x_i}\right) - \rho c_p \overline{\theta u_i}\right]. \tag{8}$$

Assuming incompressible flow, constant physical properties and neglecting additional source terms (such as radiation), the equation can be written as below:

$$\frac{DT}{Dt} = \frac{\partial}{\partial x_i}\left[\left(\frac{\nu}{Pr}\frac{\partial T}{\partial x_i}\right) - \overline{\theta u_i}\right]. \tag{9}$$

The quantity $\overline{\theta u_i}$ on the right hand side is called turbulent heat flux and is the Reynolds-averaged fluctuating velocity-temperature correlation. This quantity needs to be modeled in order to close the equation.

2.3 Turbulent Heat Flux

As previously mentioned, the heat flux must be determined to close the energy equation. The exact transport equation for $\overline{\theta u_i}$ for incompressible non-buoyant flows in the Reynolds Averaged Navier Stokes equation (RANS)-framework reads as below [15]:

$$\frac{D\overline{\theta u_i}}{\partial t} = \underbrace{\frac{\partial}{\partial x_k}\left(-\overline{\theta u_i u_k} + \frac{\overline{\theta p}}{\rho}\delta_{ik} + \nu\theta\overline{\frac{\partial u_i}{\partial x_k}} + \alpha\overline{u_i\frac{\partial \theta}{\partial x_k}}\right)}_{D_{\theta i}} + \underbrace{\overline{\frac{p}{\rho}\frac{\partial \theta}{\partial x_i}}}_{\Phi_{\theta i}} - \underbrace{\left(\overline{u_i u_k}\frac{\partial T}{\partial x_k} + \overline{\theta u_k}\frac{\partial U_i}{\partial x_k}\right)}_{P_{\theta i}} - \underbrace{(\nu+\alpha)\overline{\frac{\partial u_i}{\partial x_k}\frac{\partial \theta}{\partial x_k}}}_{\varepsilon_{\theta i}}, \quad (10)$$

where $D_{\theta i}$ is the diffusive transport, $\Phi_{\theta i}$ is the pressure-temperature correlation, $P_{\theta i}$ is the production due to combined actions of mean velocity and mean temperature gradient, and $\varepsilon_{\theta i}$ is the dissipative correlation/destruction term. The direct application of this equation to predict the heat flux is not possible due to existing of several terms that are not know ($D_{\theta i}$, $\Phi_{\theta i}$ and $\varepsilon_{\theta i}$), and need to be modeled. Explicit and implicit algebraic methods are among strategies to model this equation and will be discussed in detail in this study. Thereby, it will be explained how the unknown terms are treated and modeled.

2.3.1 Mechanical and Thermal Time Scales

There are three time scales i.e., mechanical, thermal, and a combination out of the mechanical and thermal (denoted as mixed time scale), that can be relevant to capture the turbulent thermal field at an acceptable level of accuracy and fidelity. The mechanical time scale is defined as the ratio of the turbulent kinetic energy k and its dissipation ε:

$$\tau_m = \frac{k}{\varepsilon}. \quad (11)$$

The thermal time scale follows the same principle and is represented by the ratio of the temperature variance $\overline{\theta^2}$ and its dissipation ε_θ:

$$\tau_\theta = \frac{\overline{\theta^2}}{2\varepsilon_\theta}. \quad (12)$$

However, in contrast to the mechanical time scale, this quantity cannot be obtained directly from the flow field and requires data on $\overline{\theta^2}$ and ε_θ to be obtained from corresponding transport equations discussed in Section 2.3.2.

The combined time scale τ is a combination of both time scales:

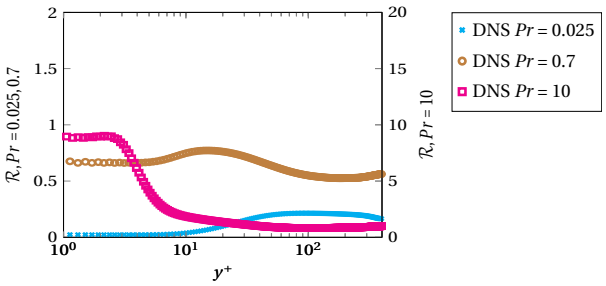

Figure 1: Ratio of thermal to mechanical time scale in turbulent channel flow for different Prandtl numbers obtained from DNS data [13]

$$\tau = \sqrt{\frac{k}{\varepsilon}\frac{\overline{\theta^2}}{\varepsilon_\theta}}. \tag{13}$$

As mentioned above, two more transport equations for $\overline{\theta^2}$ and ε_θ are necessary to calculate this time scale. However, often an overly simplistic assumption that avoids an additional transport equation for ε_θ is used. This approach assumes a constant thermal to mechanical time scale ratio, denoted as $\mathcal{R} = \tau_\theta/\tau_m$, to provide information on the thermal time scale. With the typical value of $\mathcal{R} = 0.5$ [36, 16], it results in an algebraic expression for ε_θ:

$$\varepsilon_\theta = \frac{\varepsilon\overline{\theta^2}}{k}. \tag{14}$$

Moreover, applying this simplification into the mixed time-scale, Eq. 13, leads to the mechanical time scale:

$$\tau = \sqrt{\frac{k}{\varepsilon}\frac{\overline{\theta^2}}{\varepsilon_\theta}} \overset{\text{Eq. 14}}{=} \frac{k}{\varepsilon}. \tag{15}$$

Several studies [17, 37, 18] have shown that this assumption is appropriate for fluids with Pr number around unity, but has difficulty when used to predict the thermal field of fluids with non-unity Pr numbers [42, 31]. Fig. 1 depicts dynamics of $\mathcal{R}$ in a turbulent channel flow for different Pr numbers based on Direct Numerical Simulation (DNS) data. It can be seen that this assumption could be considered as appropriate only for fluids with Pr number around unity.

2.3.2 Temperature Variance and its Dissipation

Modeling of the equation for temperature variance $\overline{\theta^2}$ is relatively straightforward and the modeled equation reads as below [36]:

$$\frac{D\overline{\theta^2}}{Dt} = 2P_\theta - 2\varepsilon_\theta + \frac{\partial}{\partial x_i}\left[\left(\frac{\nu}{Pr} + \frac{\nu_t}{\sigma_\theta}\right)\frac{\partial\overline{\theta^2}}{\partial x_i}\right], \tag{16}$$

where $P_\theta = -\overline{\theta u_i}\partial T/\partial x_i$ is the production of temperature variance. Details on model constants are provided in [36]. It should be noted that σ_θ denotes the turbulent Pr number, usually and here taken constant equal to 0.9. However, the turbulent Pr number is especially for low Pr numbers neither constant nor close to 0.9 [14]. However, an investigation of the influence of a non-constant turbulent Pr number is a complex topic and is not scope of this paper.

Modeling ε_θ is more complex compared to closing the equation for the dissipation of turbulent kinetic energy ε. As stated in [36, 20, 38, 30, 8, 24], twice as many free parameters need to be determined. Several models have been proposed [27, 18, 24, 30] which follow the same modeling methodology as for ε. This leads to the following general form for the transport equation for ε_θ [18]:

$$\frac{D\tilde{\varepsilon}_\theta}{Dt} = \mathcal{D}_{\varepsilon_\theta} + C^\theta_{\varepsilon 1} P_\theta \frac{\tilde{\varepsilon}_\theta}{\overline{\theta^2}} + C^\theta_{\varepsilon 3} P_k \frac{\tilde{\varepsilon}_\theta}{k} - C^\theta_{\varepsilon 4}\frac{\tilde{\varepsilon}^2_\theta}{\overline{\theta^2}} - C^\theta_{\varepsilon 5} f_{\varepsilon\theta}\frac{\tilde{\varepsilon}_\theta\tilde{\varepsilon}}{k} + \underbrace{E_\theta}_{\substack{\text{near-wall}\\ \text{correction}}}, \tag{17}$$

where

$$P_k = -\overline{u_i u_j}\frac{\partial U_i}{\partial x_j}, \quad P_\theta = -\overline{\theta u_i}\frac{\partial T}{\partial x_i}, \quad E_\theta = 2\alpha\alpha_t\left(\frac{\partial^2 T}{\partial x_j \partial x_k}\right)^2, \quad \tilde{\varepsilon}_\theta = \varepsilon_\theta - \underbrace{\alpha\left(\frac{\partial\sqrt{\overline{\theta^2}}}{\partial x_k}\right)^2}_{\substack{\varepsilon_\theta \text{ at}\\ \text{the wall}}}.$$

Note that the model differs in near-wall correction and ε_θ at the wall. The model proposed in [18] will be used in this study with E_θ and $\tilde{\varepsilon}_\theta$ as defined above.

2.3.3 Implicit Heat Flux Model

The implicit heat flux model takes advantage of existing known terms (particularly the production term $P_{\theta i}$) in the transport equation for the heat flux (Eq. 10). Application of the weak

equilibrium hypothesis [33, 9] along with neglecting the destruction term $\varepsilon_{\theta i}$, leaves only the pressure scrambling term $\Phi_{\theta i}$ to model. The most common method to model this term is proposed in [6, 15]:

$$\Phi_{\theta i} = -\frac{1}{\tau}\left[\frac{1}{C_{t0}}\overline{\theta u_i} + C_{t4} a_{ij}\overline{\theta u_j}\right], \tag{18}$$

where $a_{ij} = \overline{u_i u_j}/k - 2/3\delta_{ij}$. The above model for $\Phi_{\theta i}$ results in the following form for implicit algebraic turbulent heat flux model:

$$\overline{\theta u_i} = -C_{t0}\tau\left[C_{t1}\overline{u_i u_j}\frac{\partial T}{\partial x_j} + C_{t2}\overline{\theta u_j}\frac{\partial U_i}{\partial x_j}\right] + C_{t4}C_{t0}a_{ij}\overline{\theta u_j}. \tag{19}$$

As mentioned before, the time scale τ is the mixed time scale that requires information of $\overline{\theta^2}$ and ε_θ. However, investigations concerning turbulent wall-bounded shear flows [36, 34, 16] use a simplified version of the model based on the constant thermal to mechanical time scale assumption with $\mathcal{R} = 0.5$. The simplified form of the model reads as follows:

$$\overline{\theta u_i} = -C_{t0}\frac{k}{\varepsilon}\left[C_{t1}\overline{u_i u_j}\frac{\partial T}{\partial x_j} + C_{t2}\overline{\theta u_j}\frac{\partial U_i}{\partial x_j}\right] + C_{t4}C_{t0}a_{ij}\overline{\theta u_j}. \tag{20}$$

Further, it was shown [36] that the model constants need to be modified to reach an acceptable level of accuracy for differnt Pr numbers, leading to a correlation for C_{t1}. This resulting model is referred to as *AHFM-NRG*, and will be used in this investigation. Model coefficients are summarized in Tab. 1.

C_{t0}	C_{t1}	C_{t2}	C_{t4}
0.2	0.053 ln $(RePr)$-0.27	0.6	0.0

Table 1: Coefficients for the implicit heat flux model *AHFM-NRG* as given by [36]
pdflatex

It should be noted that all previously mentioned studies that use the *AHFM-NRG* model are limited to fluids with Pr numbers around or less than unity and do not provide data on some relevant statistical quantities such as the heat fluxes. Moreover, they do not address the sensitivity of the heat flux model with respect to the turbulence model used to described the flow field.

In this study, the *AHFM-NRG* model will be assessed extensively when applied to turbulent (attached) wall-bounded shear flows of different working fluid. Additionally, the *AHFM-NRG*

model will be modified by incorporating the thermal time scale into the model, i.e. the mechanical time scale will be replaced by the mixed time scale. This will allow to identify relevance of the thermal time scale, as well as, if/how the implicit modeling methodology responds to the inclusion of the thermal time scale.

2.3.4 Explicit Heat Flux Model

An explicit model for turbulent heat flux can be constructed based on the representation theorem. Assuming an incompressible, non-buoyant flow at high Reynolds numbers, the functional relationship for the turbulent heat flux is given as below [40]:

$$\overline{\theta u_i} = -f_i\left(\overline{u_i u_j}, S_{ij}, W_{ij}, T_{,j}, T, \varepsilon, \overline{\theta^2}\right), \tag{21}$$

where S_{ij} is the mean rate of strain and W_{ij} is the mean vorticity tensor.

For the determination of the model, it is assumed that anisotropies and turbulent time-scales are sufficiently small and that an equal balance between the effects of rotational and irrotational strain rates exists. Further details including a detailed derivation of the model are provided in [40]. The model reads as follows:

$$\overline{\theta u_i} = -\left[C_1\tau_e k\frac{\partial T}{\partial x_i} + C_2\tau_e\overline{u_i u_j}\frac{\partial T}{\partial x_j} + C_3\tau_e^2 k\frac{\partial U_i}{\partial x_j}\frac{\partial T}{\partial x_j} + C_4\tau_e^2\left(\overline{u_i u_k}\frac{\partial U_j}{\partial x_k} + \overline{u_j u_k}\frac{\partial U_i}{\partial x_k}\right)\frac{\partial T}{\partial x_j}\right]. \tag{22}$$

Here, τ_e can represent either the mechanical or thermal or mixed time scale. Choosing the mechanical time scale (following the same assumption as for the implicit flux model, a constant ratio between mechanical and thermal time scale with $\mathcal{R} = 0.5$) leads to the proposed model in Younis et al. [40]:

$$\overline{\theta u_i} = -\left[C_1\frac{k^2}{\varepsilon}\frac{\partial T}{\partial x_i} + C_2\frac{k}{\varepsilon}\overline{u_i u_j}\frac{\partial T}{\partial x_j} + C_3\frac{k^3}{\varepsilon^2}\frac{\partial U_i}{\partial x_j}\frac{\partial T}{\partial x_j} + C_4\frac{k^2}{\varepsilon^2}\left(\overline{u_i u_k}\frac{\partial U_j}{\partial x_k} + \overline{u_j u_k}\frac{\partial U_i}{\partial x_k}\right)\frac{\partial T}{\partial x_j}\right]. \tag{23}$$

This model has not been tested in fully attached turbulent boundary layers. However, there is a recent investigation [26] that employs a slightly modified version to study non-isothermal rotating and non-rotating turbulent channel flow. The modified model reads as follows:

$$\overline{\theta u_i} = -\left[C_1 \frac{k^2}{\varepsilon} \frac{\partial T}{\partial x_i} + C_2 \frac{k}{\varepsilon} \overline{u_i u_j} \frac{\partial T}{\partial x_j} + C_4 \frac{k^2}{\varepsilon^2} \left(\overline{u_i u_k} \frac{\partial U_j}{\partial x_k} - \overline{u_j u_k} \frac{\partial U_i}{\partial x_k} \right) \frac{\partial T}{\partial x_j} \right]. \tag{24}$$

While this model offers remarkable improvements compared to the classical Reynolds Analogy based model, it is worth noting that only the mechanical time scale was included as well as only working fluids with Pr around unity were tested. This modified model will be used in this study and the model coefficients are given in Tab. 2.

C_1	C_2	C_3	C_4
0.03	0.21	0.0	-0.105

Table 2: Coefficients for the explicit heat flux model as given by [26]

Moreover, similar to the implicit heat flux model, sensitivity of the model with respect to the turbulence model and effect of considering the thermal time scale will be investigated. Inclusion of the thermal time scale into the model and using the mixed time scale will result in the following form of the model:

$$\overline{\theta u_i} = -\left[C_1 \tau k \frac{\partial T}{\partial x_i} + C_2 \tau \overline{u_i u_j} \frac{\partial T}{\partial x_j} + C_4 \tau^2 k \left(\overline{u_i u_k} \frac{\partial U_j}{\partial x_k} - \overline{u_j u_k} \frac{\partial U_i}{\partial x_k} \right) \frac{\partial T}{\partial x_j} \right]. \tag{25}$$

It should be noted that the model constants remain same after modifying the time scale, as discussed in the introduction.

3 Numerical Setup

3.1 Flow Configuration

The configuration is a fully developed turbulent channel flow as shown in Fig. 2. The size of the computational domain is $2\pi\delta, 2\delta, \pi\delta$, where δ is the channel half height. Different Prandtl numbers (0.025, 0.71, 10) have been considered based on the availability of reference (DNS) data. The details of all simulations are summarized in table 3.

Different mesh designs have been used for different Prandlt numbers and in particular, a different spacing in wall-normal direction is required to achieve appropriate distribution according to the findings in [42]. A simple-gradient spacing is used to create suitable distributions in the wall-normal direction, see [29]for details.

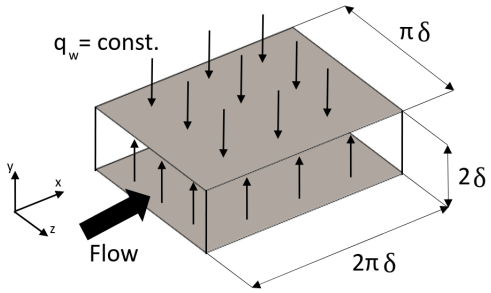

Figure 2: Sketch of horizontal channel flow configuration

Note that the Reynolds number $Re_\tau = U_\tau \delta/\nu$ is defined based on the friction velocity at wall (U_τ) and channel half height δ. A constant pressure gradient is applied via an additional source term in the momentum equation to drive the flow to the targeted Reynolds number.

Periodic boundary conditions are imposed in the streamwise and spanwise directions, and no-slip condition is used at both walls. For the temperature field, a mean uniform heat flux at the walls, and periodic boundary conditions in the streamwise and the spanwise directions have been applied. Further, it is important to mention that the temperature variance and its dissipation are set to zero at the wall, i.e. $\overline{\theta^2}|_w$ and $\varepsilon_\theta|_w = 0$. The results are normalized by the δ, U_τ, the kinematic viscosity ν, the density ρ, and the friction temperature T_τ.

Three different model categories for the thermal field will be applied and assessed in this investigation. These include *TV-R*, *TV-E* and *TV-M*. *TV-R* uses solely the mechanical time scale along with the transport equation for $\overline{\theta^2}$, (Eq. 16), and the algebraic expression to determine ε_θ, (Eq. 14), for both the implicit and explicit heat flux model. *TV-E* makes use of the transport equation for ε_θ, (Eq. 17), to provide information for thermal dissipation while using only the mechanical time scale similar to category *TV-R*. The last category (*TV-M*) takes leverage of the mixed time scale τ defined by Eq. 13 in both turbulent heat flux models. All three categories along with corresponding equations are summarized in Tab. 4. It should be noted that the heat flux calculations in categories *TV-R* and *TV-E* are independent of the results obtained for $\overline{\theta^2}$ and ε_θ. However, these two quantities are solved as well for further analysis about second order thermal statistics.

Re_τ	Pr	Resolution	Reference data
395	0.025, 0.7, 10	$48 \times 36 \times 6$	Kawamura et al. [12]

Table 3: Overview of flow and fluid properties

category	$\overline{\theta u_i}$-Equation		time scale	$\overline{\theta^2}$-Equation	ε_θ-Equation
	Implicit	Explicit			
TV-R	Eq. 20	Eq. 24	$\frac{k}{\varepsilon}$	Eq. 16	Eq. 14
TV-E	Eq. 20	Eq. 24	$\frac{k}{\varepsilon}$	Eq. 16	Eq. 17
TV-M	Eq. 19	Eq. 25	$\sqrt{\frac{k}{\varepsilon}\frac{\overline{\theta^2}}{\varepsilon_\theta}}$	Eq. 16	Eq. 17

Table 4: Overview of model categories

3.2 Code Description

All numerical simulations presented in this publication are performed using OpenFOAM-v2.2.2 with necessary modifications for the purpose of this paper. The PISO-algorithm has been used and second order schemes have been applied for velocity, turbulence and thermal quantities.

3.3 Validation and Comparison of Turbulence Models

In this section, two turbulence models used in this investigation will be assessed and compared when applied to a fully developed turbulent channel flow. Mesh convergence studies have been done for all simulations and only mesh independent results are presented. All simulations have been conducted in steady state fashion using RANS based turbulence models described in section 2.1. Mean velocity, turbulent kinetic energy and its dissipation are shown in Fig. 3. It can be seen, that the velocity is well predicted by both models. Turbulent kinetic energy k is better predicted by *LA* model in the peak-region, while the near-wall region is underpredicted by both models. The dissipation of turbulent kinetic energy (ε) is predicted with the same accuracy, however, with a strong underprediction in the wall- region, while the mechanical time scale that enters the turbulent heat flux models is fairly well predicted.

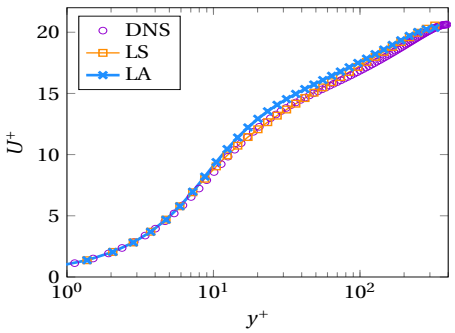

(a) Mean velocity

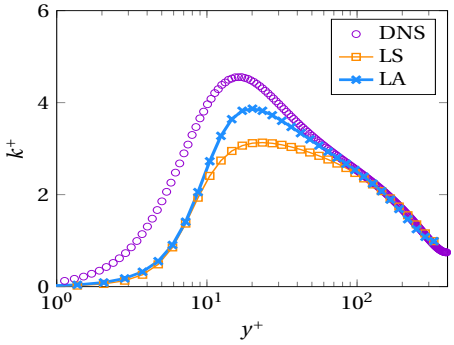

(b) Turbulent kinetic energy

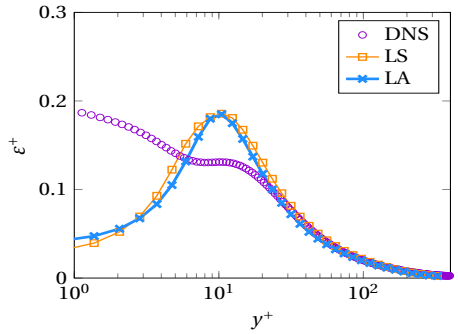

(c) Dissipation of turbulent kinetic energy

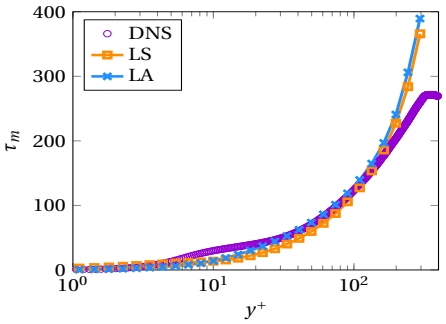

(d) Mechanical time scale

Figure 3: Re_τ= 395. Flow quantities

The Reynolds stresses play integral roles in prediction of the turbulent heat fluxes, as can be deduced from the governing equations (Eqs. 19 and 25). Fig. 4 demonstrates these Reynolds stresses obtained from the two turbulence models. It can be observed that the normal stresses ($\overline{uu}, \overline{vv}, \overline{ww}$) are remarkably better predicted by the non-linear model (*LA*). It should be noted that other components of the Reynolds stress tensor ($\overline{uw}, \overline{vw}$) also enter the heat flux equations in more complex configurations, however, they are zero for the test case considered here.

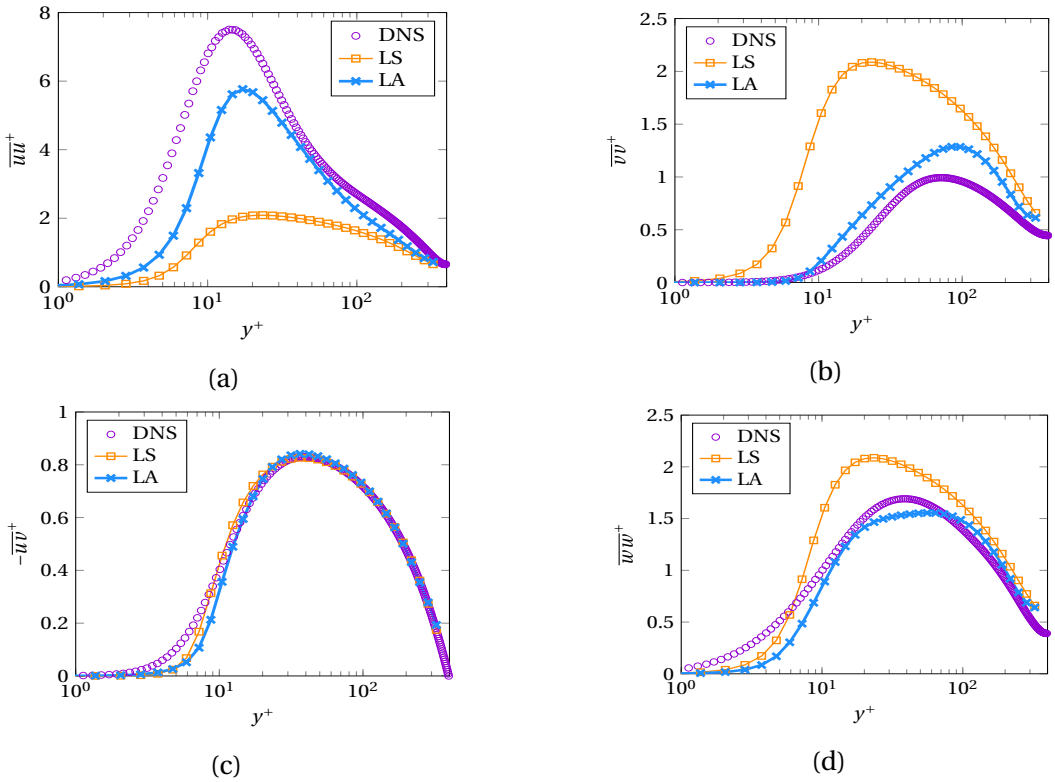

Figure 4: $Re_\tau = 395$. Reynolds Stresses

4 Results and Discussion

4.1 $Pr = 0.71$

Fluids with Prandtl numbers around unity differ strongly in their behavior compared to high and low Pr number fluids. In particular, the thermal and momentum boundary layers overlay for fluids with Pr number around unity and thus, a constant value (usually 0.5) for the ratio of mechanical to thermal time scale works reasonably well, as also shown in [17, 37, 18]. It follows that considering the thermal time scale in the heat flux model may not provide remarkable modifications, i.e. results from all three model categories (*TV-R*, *TV-E* and *TV-M*) share a lot of similarity. Therefore, only thermal quantities that are significantly affected by the inclusion will be demonstrated and discussed.

4.1.1.1 Mean Temperature

Fig. 5 presents mean temperatures obtained for Pr = 0.71 at Re_τ = 395 for *TV-R* and *TV-E*. It should be noted that both models result in the same temperature profile, since the temperature equation is independent of $\overline{\theta^2}$ and ε_θ, see section 2.3.3. The mean temperature is not well captured, irrespective of the turbulence model used to capture the flow field. It appears that while the implicit model is sensitive to the flow field prediction (linear vs. non-linear turbulence model), it does not respond in a consistent manner to improvements of flow field quantities such as the Reynolds stresses, provided by the non-linear turbulence model (*LA*). This behavior of the model is somehow peculiar since one of the key elements of the model, i.e. the Reynolds stress tensor (particularly $\overline{vv}$), is better predicted when the non-linear turbulence model is used. Furthermore, misprediction of the mean temperature traces back to inaccuracy in prediction of the wall-normal heat flux, which also responds inconsistently to the flow field prediction accuracy (Fig. 6). This might be indicative of model inability to establish a consistent coupling with the flow field. This may suggest that the current version of the model proposed by [36] has been calibrated/tuned for the specific turbulence model used in the investigation, which makes the model less reliable for general applications.

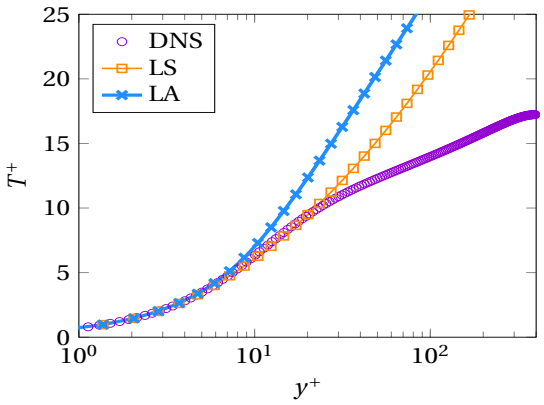

Figure 5: Mean temperature obtained by *TV-R* and *TV-E* for Pr= 0.71 at Re_τ= 395 with the implicit heat flux model and the two shear stress models *LS* and *LA*

4.1.1.2 Streamwise and Wall-Normal Heat Flux

The streamwise and wall-normal heat fluxes obtained by *TV-R* and *TV-E* approaches are shown in Fig. 6. Similar to mean temperature, the heat fluxes are independent of temperature variance and its dissipation. The streamwise heat flux is strongly mispredicted by the implicit heat flux model regardless of the turbulence model used to provide flow field quantities. In fact, there is only little sensitivity to the heat flux in the homogeneous direction. In contrast, the implicit model is at least capable of capturing the overall behavior of the wall-normal heat flux, however with an underprediction of the peak. It is worth noting that it seems that the near-wall region is better predicted with the linear turbulence model. However, this is deemed to be an accident, given the lower prediction quality of the Reynolds stresses and in particular $\overline{vv}$, which is the major contributor to the heat fluxes, Eq. 20.

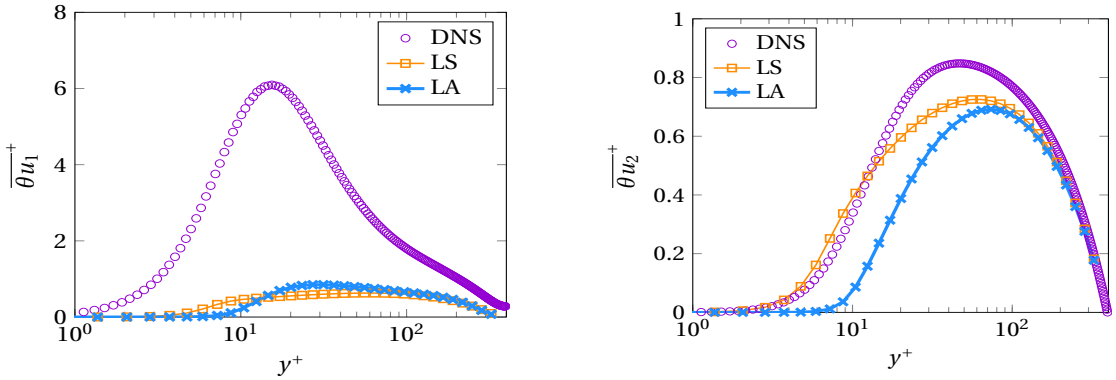

(a) *TV-R* and *TV-E*

(b) *TV-R* and *TV-E*

Figure 6: Streamwise (a) and wall-normal (b) heat fluxes obtained by *TV-R* and *TV-E* for Pr= 0.71 at Re_τ= 395 with the implicit heat flux model

4.1.1.3 Temperature Variance

Unlike the mean temperature and heat fluxes, there are differences in results obtained by *TV-E* and *TV-R* for temperature variance (equivalently, the root mean square (rms) value of temperature fluctuations denoted as θ_{rms}), see Section 3. Regarding *TV-R*, irrespectively of the turbulence model, the implicit heat flux model fails to capture the general behavior of θ_{rms}, see Fig. 7a. Using an extra transport equation for the thermal dissipation ε_θ (*TV-E*) does not provide improvements, compared to *TV-R*, while exacerbates the situation in the core region. The discrepancies trace back to two effects: first, misprediction of mean temperature and heat fluxes (Fig. 5 and 6), since mean temperature gradient and heat fluxes

are major contributors in production of $\overline{\theta^2}$, as shown in Eq. 16. Secondly, k is mispredicted in the wall region by both turbulence models as discussed previously. This quantity enters the transport equation for $\overline{\theta^2}$ by means of ν_t, which may negatively impact the prediction accuracy. Additionally, σ_θ in Eq. 16 is considered to be constant. However, according to DNS data [14] this quantity varies in the wall-region but to study the effects of variable σ_θ is not within the scope of the present investigation.

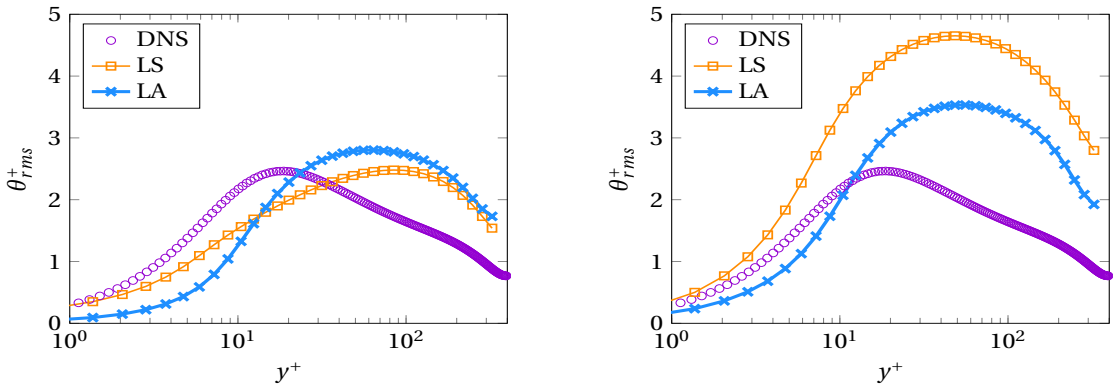

(a) *TV-R* (b) *TV-E*

Figure 7: Temperature rms obtained by *TV-R* and *TV-E* for Pr= 0.71 at Re_τ= 395 with the implicit heat flux model

4.1.2 Explicit Heat Flux Model

4.1.2.1 Mean Temperature

In Fig. 8, the mean temperatures obtained by the explicit heat flux model using both turbulence models within *TV-R* and *TV-E* approaches are shown. The result using the linear turbulence model (*LS*) underestimate the profile strongly, which is due to the overestimation of the wall-normal heat flux, Fig. 9c, while the result using the non-linear turbulence model (*LA*) is in good agreement with the reference data, consistent with prediction accuracy of the wall-normal heat flux in the wall region. More importantly, in comparison to the implicit heat flux model, the explicit heat flux model shows a consistent sensitivity to the turbulence model, i.e. the more accurate the Reynolds stresses, the more accurate the thermal field.

4.1.2.2 Streamwise and Wall-Normal Heat Flux

Fig. 9 shows the streamwise and wall-normal heat fluxes obtained by *TV-R*, *TV-E* and *TV-M*. In contrast to the implicit model (Fig. 6 a), the explicit heat flux model demonstrates

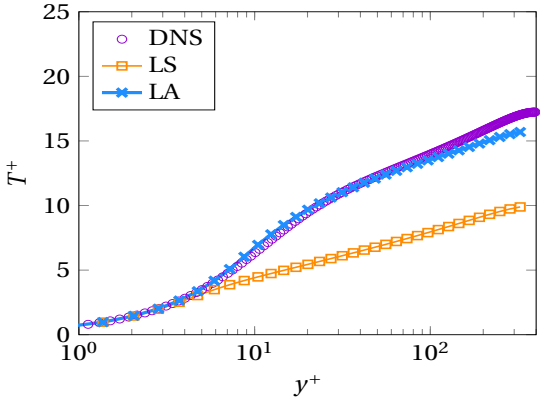

Figure 8: Mean temperature obtained by *TV-R* and *TV-E* for Pr= 0.71 at Re_τ= 395 with the explicit heat flux model

potential capability to capture the streamwise heat flux, see Fig. 9a. In particular, the model shows a decent capability, when the non-linear turbulence is used. This positive response is also present in the mean temperature. This may suggest that an accurate prediction of the flow field along with an appropriate model for the heat flux are essential to address the shortcomings of heat flux models in predicting heat fluxes in homogeneous directions. Fig. 9c depicts the wall-normal heat fluxes obtained by *TV-R* and *TV-E*. It can be observed that the wall-normal heat flux can be accurately predicted, if the non-linear turbulence model (*LA*) is used.

Using the mixed time scale (*TV-M*) offers improvements for the streamwise heat flux (Fig. 9b). In particular, thermal time scale appears to play an integral role in predicting second order statistics in the core region. Additionally, the discrepancy in the near-wall region is thought to be due the inaccurate prediction of the turbulent kinetic energy in this region, as discussed before.

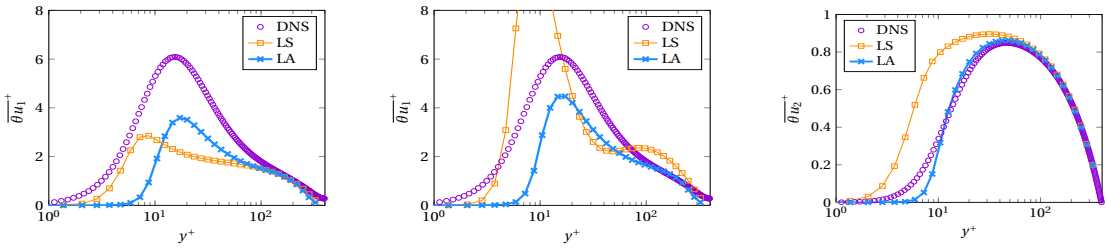

(a) *TV-R* (b) *TV-M* (c) *TV-R* and *TV-E*

Figure 9: Streamwise (a) and (b), and wall-normal (c) heat fluxes obtained for Pr= 0.71 at Re_τ= 395 with the explicit heat flux model

4.1.2.3 Temperature Variance

Temperature variances (θ_{rms}) obtained by *TV-R* and the explicit heat flux model are shown in Fig. 10a. As can be seen, the explicit model shows sensitivity to the accuracy of the flow field. Inclusion of an extra transport equation for ε_θ , i.e. *TV-E*, seems to affect the results obtained with both turbulence models, leading to overall improvements, see Fig. 10b. This demonstrates that providing more accurate data on the thermal time scale (i.e. considering an extra transport equation for ε_θ) appears to be at least partially relevant to capture near-wall dynamics accurately. The inaccuracy in the wall-region could be due to existing inaccuracy in prediction of the turbulent kinetic energy (k) in this region and potentially, considering constant σ_θ.

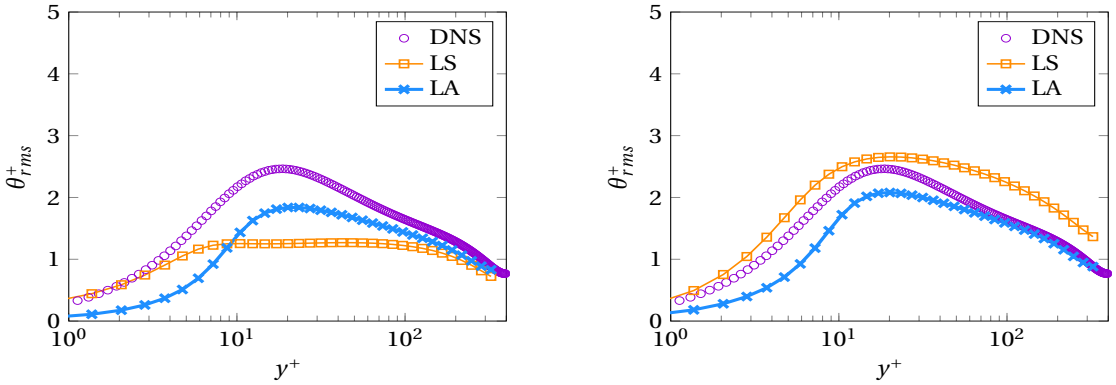

(a) *TV-R* (b) *TV-E*

Figure 10: Temperature rms obtained by *TV-R* and *TV-E* for Pr= 0.71 at Re_τ= 395 with the explicit heat flux model

4.2 Pr= 0.025 AND EXPLICIT HEAT FLUX MODEL

In contrast to fluids with Pr numbers around unity, thermal boundary layers of fluids with Pr numbers substantially less than unity show different characteristics compared to the velocity (hydrodynamics) boundary layer. In particular, thermal boundary layers of low Pr number fluids are thicker than hydrodynamic boundary layers, leading to much smaller thermal time scales as shown in Fig. 1. It should be noted that, for brevity of the paper, results obtained using the implicit model will not be shown as the model fails completely to capture essential thermal quantities, i.e., the streamwise and wall-normal heat fluxes, that leads to misprediction of other quantities. In particular, the model shows almost no sensitivity

to the heat fluxes in both directions, although the model is expected to be able dealing with low Pr number fluids [36, 34]. Furthermore, the model fails to respond consistently to the improvement of the flow field prediction provided by the non-linear turbulence model, similar to what was observed for the previous case (Pr=0.71).

4.2.1 Mean Temperature

The mean temperatures obtained with both turbulence models using the explicit heat flux model within *TV-R*, *TV-E* and *TV-M* approaches are shown in Fig. 11. The results obtained with both turbulence models underestimate mean temperature in the core region of the channel, consistent with overprediction of wall-normal heat flux in this region, Fig. 13. Inclusion of the thermal time scale in conjunction with the non-linear turbulence model offers some improvement pointing to potential relevance of the thermal time scale.

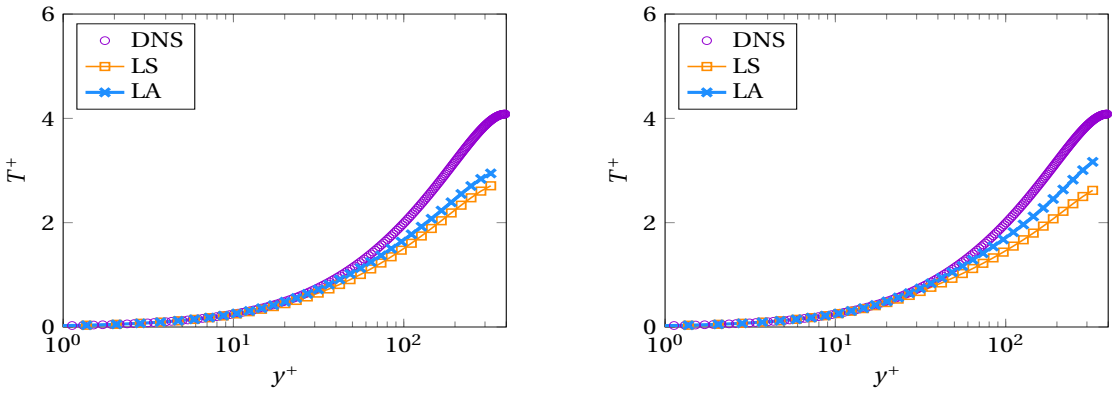

(a) *TV-R* and *TV-E* (b) *TV-M*

Figure 11: Mean temperature obtained by *TV-R*, *TV-E* and *TV-M* for Pr= 0.025 at Re_τ= 395 with the explicit heat flux model

4.2.2 Streamwise and Wall-Normal Heat Flux

Fig. 12a shows the streamwise heat fluxes obtained by *TV-R* and *TV-E* using both turbulence models. The explicit heat flux model shows some degree of sensitivity to the heat flux in the streamwise direction (in contrast to the implicit model). However, the flux is strongly overpredicted, which leads to misprediction of other thermal quantities.

Including the mixed time scale (*TV-M*) offers somehow improvements to capture the general behavior of the heat flux (Fig. 12b), demonstrating promising potential of explicit framework for reliable prediction of thermal quantities. In particular, results are indicative of

relevance of thermal time scale to capture second order statistics thermal field for fluids with Pr numbers other than unity. However, there are still remarkable deviations from reference data in the core region, which is thought to be due to inaccuracy in predicting the thermal time scale, given that the flow quantities are fairly well predicted in this region.

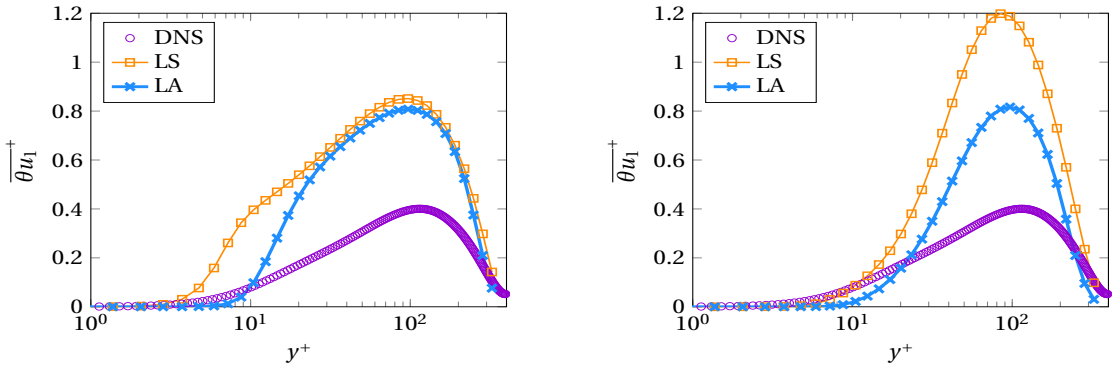

(a) *TV-R* and *TV-E* (b) *TV-M*

Figure 12: Streamwise heat flux obtained by *TV-R*, *TV-E* and *TV-M* for $Pr = 0.025$ at $Re_\tau = 395$ with the explicit heat flux model

Wall-normal flux obtained from *TV-R*, *TV-E* and *TV-M* is shown in Fig. 13. All approaches are capable of capturing the general trend in the core region, particularly when the non-linear turbulence model was used. Nevertheless, the profile is strongly overpredicted.

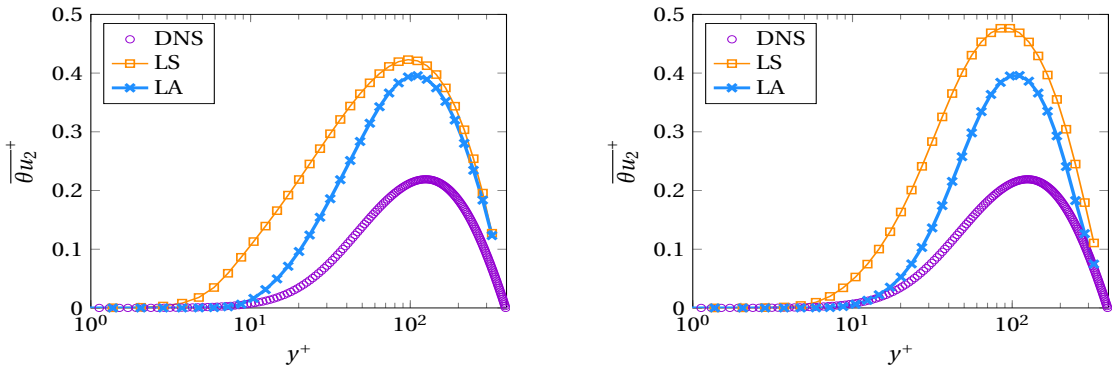

(a) *TV-R* and *TV-E* (b) *TV-M*

Figure 13: Wall-normal heat flux obtained by *TV-R*, *TV-E* and *TV-M* for $Pr = 0.025$ at $Re_\tau = 395$ with the explicit heat flux model

4.2.3 Temperature Variance

Temperature variances (θ_{rms}) obtained by *TV-R* and the explicit heat flux model are shown in Fig. 14a. As can be seen, the explicit model shows no sensitivity to the accuracy of the

flow field but captures the trend of θ_{rms} accurately. However, there is overprediction present which is thought to trace back to inaccurate predictions of heat fluxes and thermal dissipation. Inclusion of an extra transport equation for ε_θ (*TV-E*) seems to affect the results obtained with both turbulence models, most notably when the Reynolds stresses are predicted at a higher level of accuracy, Fig. 14b. Inclusion of the mixed time scale shows only slight improvements close to the channel core when the non-linear turbulence model was applied, Fig. 14c.

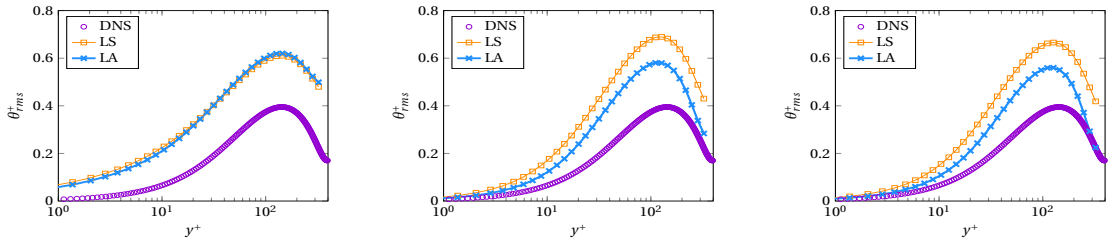

(a) *TV-R* (b) *TV-E* (c) *TV-M*

Figure 14: Temperature rms obtained by *TV-R*, *TV-E* and *TV-M* for $Pr = 0.025$ at $Re_\tau = 395$ with the explicit heat flux model

4.2.4 Dissipation of Temperature Variance

Thermal dissipation (ε_θ) plays an important role to accurately predict the temperature variance, as well as heat fluxes when the thermal time scale is considered. Results for the dissipation of temperature variance obtained for *TV-R* are presented in Fig. 15a. The profiles obtained with both turbulence model mostly differ in near-wall region ($y^+ < 100$), while fail to capture the plateau behavior. Some improvement regarding the general tendency of ε_θ can be observed, when an additional transport equation for ε_θ (*TV-E*) is used, most notably using the non-linear turbulence model, Fig. 15b.

Inclusion of the mixed time scale (*TV-M*) shows improvements regarding the magnitude of the captured plateau obtained with both turbulence model, Fig. 15c. The explicit model shows consistent sensitivity to the turbulence model, as well as to the inclusion of the mixed time scale. However, it should be noted that although some improvement regarding the overall behavior has been achieved, there are still significant deviation from the reference data. In particular, the location of the peak is mispredicted and has not been improved after inclusion of the mixed time scale. This can be traced back to two characteristics of the modeled ε_θ equation. First, ε and k play an integral role in the production terms of ε_θ, see Eq. 17. As shown before, both turbulence model underpredict these quantities. Secondly, these

results may suggest that ε_θ, in case of low Pr number fluids, should not be modeled solely based on similar assumptions made to model the dissipation of turbulent kinetic energy (ϵ), see Section 2.3.2 for details. Finally, inaccuracy in prediction of ε_θ and θ_{rms} leads to an inaccurate prediction of the thermal time scale contributing to misprediction of heat fluxes and ultimately other thermal quantities within *TV-M* approach.

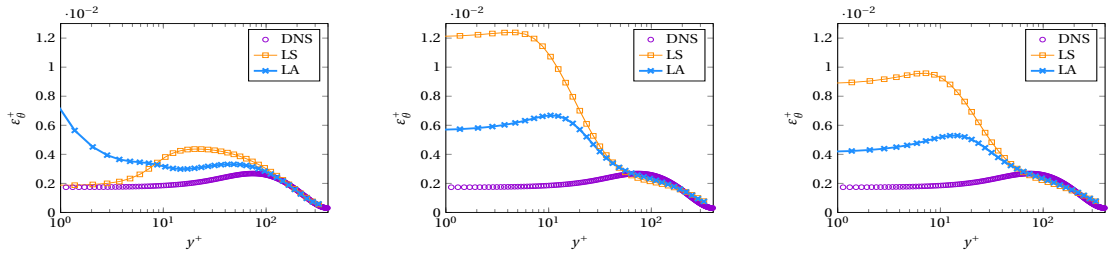

(a) *TV-R* (b) *TV-E* (c) *TV-M*

Figure 15: Dissipation of temperature variance obtained by *TV-R*, *TV-E* and *TV-M* for Pr= 0.025 at Re_τ= 395 with the explicit heat flux model

4.3 Pr= 10 AND EXPLICIT HEAT FLUX MODEL

In contrast to low Prandtl number fluids, the thermal boundary layer for high Pr number fluids is much thinner than the velocity boundary layer. This requires a different mesh design to capture dynamics of the thermal boundary layer accurately. In particular, much finer resolution is necessary in near-wall region as discussed in [42]. Moreover, it will be shown that the thermal time scale needs to be considered in order to increase the prediction accuracy of first and second order statistics such as mean temperature and temperature variance. Again, results obtained by the implicit model are not shown here as it fails to predict the thermal quantities such as mean temperature.

4.3.1 MEAN TEMPERATURE

The mean temperature obtained with *LS* underestimates the profile, while using *LA* leads to an overprediction of mean temperature, Fig. 16a. The core region is not well predicted, which traces back to the misprediction of wall-normal heat flux in the near-wall region, Fig. 17.

Introducing the thermal time scale into the explicit heat flux model has a remarkable effect on the prediction when *LA* turbulence model is used, leading to a profile that is in good agreement with the reference data, Fig. 16b. Accordingly, the wall-normal heat flux shows

some improvements, Fig. 17d. This indicates the relevance of the thermal time scale in the wall-region, as well as, accuracy of the flow field when dealing with high Pr number fluids.

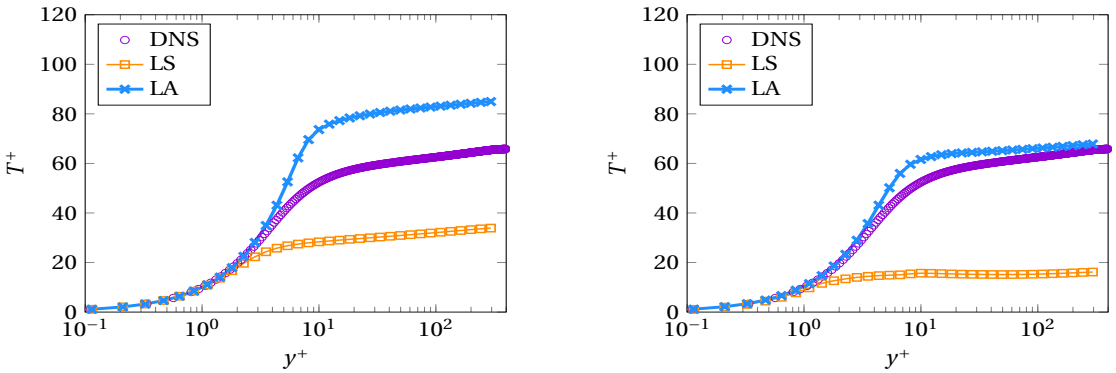

(a) *TV-R* and *TV-E* (b) *TV-M*

Figure 16: Mean temperature obtained by *TV-R*, *TV-E* and *TV-M* for Pr= 10 at Re_τ= 395 with the explicit heat flux model

4.3.2 Streamwise and Wall-Normal Heat Flux

Fig. 17a presents the streamwise heat fluxes obtained by *TV-R* and *TV-E*. Regardless of the turbulence model, the heat flux is underpredicted and leads to misprediciton of other thermal quantities.

Inclusion of the mixed time scale leads to significant improvements when the the non-linear turbulence model is used, Fig. 17b. However, it should be noted that if the flow field is not predicted at an acceptable level of accuracy, the heat flux model could potentially deliver a remarkable discrepancy or even become numerical unstable, as demonstrated here when using the linear turbulence model (*LS*).

Fig. 17c depicts the wall-normal heat fluxes obtained by *TV-R* and *TV-E*. It can be observed that the explicit heat flux model is capable to predict the wall-normal heat flux fairly accurate except for regions very close to the wall ($y^+ < 10$), irrespective of turbulence model.

Inclusion of the mixed time scale improves prediction accuracy in the near-wall region, when the non-linear turbulence model is used, Fig. 17d. As mentioned before, this leads to improvement of other thermal quantities, e.g. mean temperature. In contrast, using the linear turbulence model for the flow field leads to a significant error. Therefore, it may be deduced that the thermal time scale plays an integral role to capture the thermal field of high Pr number fluids, however, the flow field needs to be captured at a certain level of accuracy.

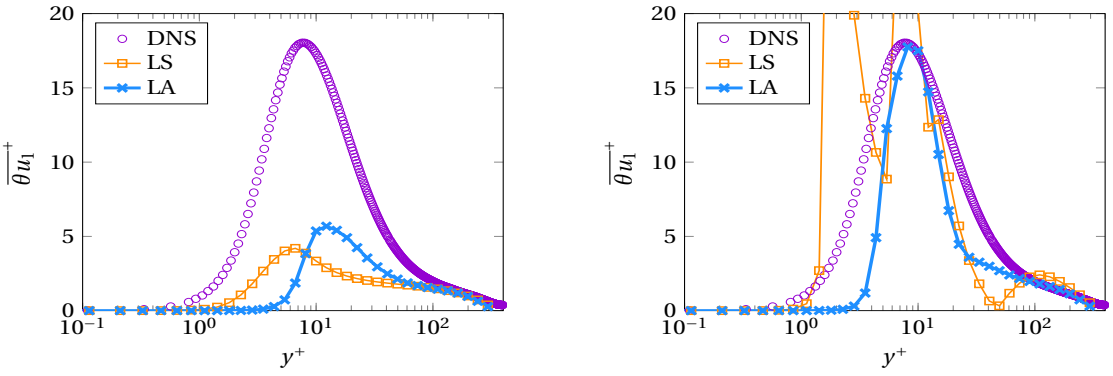

(a) *TV-R* and *TV-E*

(b) *TV-M*

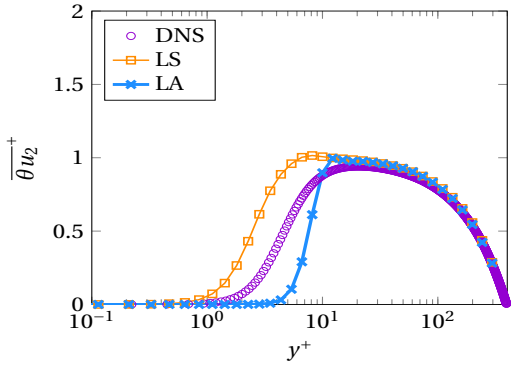

(c) *TV-R* and *TV-E*

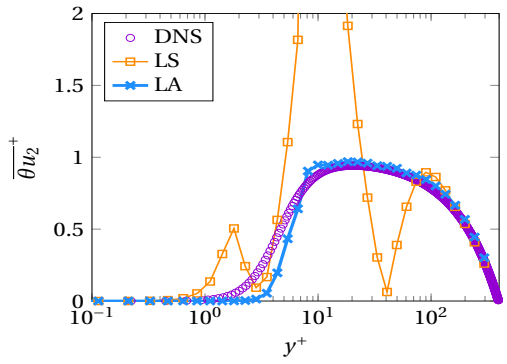

(d) *TV-M*

Figure 17: Streamwise and wall-normal heat flux obtained by *TV-R*, *TV-E* and *TV-M* for Pr= 10 at Re_τ= 395 with the explicit heat flux model

4.3.3 Temperature Variance

Temperature variances (θ_{rms}) obtained by *TV-R* and the explicit heat flux model are shown in Fig. 18a. As can be observed, the explicit model captures the general behavior with both turbulence models, however, with a significant deviation from reference data. Moreover, using an extra transport equation for ε_θ (*TV-E*) provides improvement (Fig. 18b), pointing to the different dynamics of thermal time scale compared to mechanical time scale.

Inclusion of the mixed time scale (*TV-M*) affects the results obtained with both turbulence models, Fig. 18c. While remarkable improvements can be observed for the prediction with *LA*, θ_{rms} predicted with *LS* demonstrates notable discrepancy. The accurate prediction is mainly a direct result of accurate predictions of wall-normal heat flux, as well as mean temperature, when the thermal time scale is considered in the heat flux model.

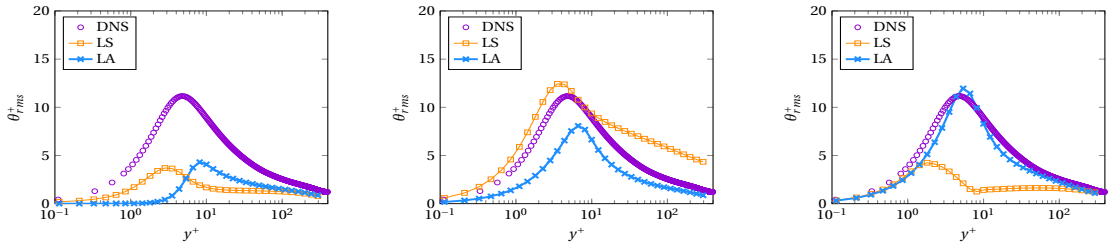

(a) *TV-R* (b) *TV-E* (c) *TV-M*

Figure 18: Temperature rms obtained by *TV-R*, *TV-E* and *TV-M* for $Pr = 10$ at $Re_\tau = 395$ with the explicit heat flux model

5 Conclusion and Outlook

The current study aims at taking a foundational step towards identification and development of a reliable framework to predict the thermal field of different fluids in turbulent wall-bounded shear flows. Therefore, the most recent versions of implicit and explicit heat flux models have been thoroughly assessed. This includes the application of the models to turbulent wall-bounded attached shear flows of different Prandtl number fluids. Further, sensitivity of both models with respect to the prediction accuracy of the flow field (mean velocity and the Reynolds stress tensor) has been studied.

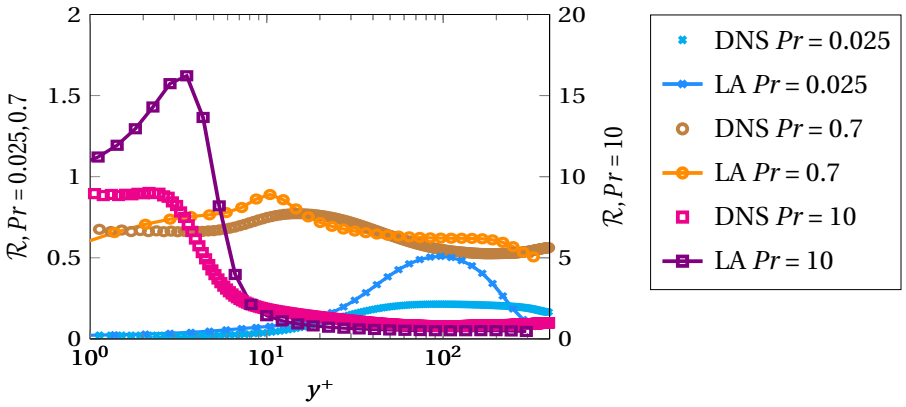

Figure 19: Best results for the ratio of thermal to mechanical time scale obtained by *TV-M*, non-linear turbulence model and explicit heat flux model for $Pr = 0.025$, 0.7 and 10 at $Re_\tau = 395$

It turns out that the *NRG* formulation (the most recent formulation) of implicit framework has difficulty to establish a consistent coupling to the flow field, which leads to inappropriate responses to the flow field prediction accuracy. As a results of this, the model is incapable of providing accurate results for thermal quantities such mean temperature, irrespective of the Pr number, even when the flow field and in particular, the Reynolds stress tensor

is accurately predicted. However, it appears that the model delivers accurate results for mean temperature for fluids with Pr numbers around unity and less, as shown in [36], if a specific turbulence model is used, for which model constants have been calibrated. However, capability of the model in predicting heat fluxes has never been demonstrated and discussed in corresponding investigations [36, 34]. This makes the model calibration to create a general and robust computation framework extremely difficult. Moreover, the implicit model used here appears to have difficulty dealing with heat flux in homogeneous directions, irrespective of the Pr number and turbulence model.

In contrast, the explicit framework indicates potential capability to deal with complex turbulent thermal fields of different working fluids. In particular, it responds consistently to the accuracy of the flow field prediction, i.e. accurate prediction of the flow field including mean quantities and the Reynolds stress tensor is required for an accurate prediction of the thermal field. The necessity of accurate prediction of the flow field becomes more crucial when near-wall effects become more relevant for high Pr number fluids. In particular, if near-wall effects (3D characteristics of turbulence) are not provided at an acceptable level of accuracy, the model fails completely. This is best shown in predictions of heat fluxes for high Pr number (Pr= 10), when the linear model (LS) was used to describe the flow field, Fig. 17. Moreover, it turns out the explicit formulation has the potential to address the main issues of heat transfer models and shows capability (sensitivity) to capture the heat flux in homogeneous directions. Additionally, inclusion of the thermal time scale to the model has shown to be necessary for accurate prediction of the thermal field of fluids with Pr number other than unity. However, currently available modeled transport equations for thermal dissipation appear to be inappropriate to be applied to fluids with Pr numbers other than unity (see the appendix for the thermal dissipation for Pr= 10 obtained from the explicit model), as it leads to inaccurate thermal time scale, which is demonstrated in Fig. 19. The results obtained here reveal that the development and modeling of thermal dissipation (as a key element of thermal time scale) in fluids with Pr numbers different than unity cannot be based on same arguments and strategies as for the flow field at high Reynolds number. Therefore, there is a need for much more in-depth investigations using high fidelity approaches (i.e., DNS) to identify and understand major dynamics of thermal dissipation in such fluids, which probably will be different for high and low Pr number fluids. However, those investigations are out of the scope of the current paper.

6 Acknowledgment

Dr. Mueller is acknowledged for providing the original source code for the explicit heat flux model. This work was supported using start-up funds from the University of Missouri-Kansas City.

7 Appendix

Dissipation of Temperature Variance for Pr=10

The explicit heat flux model provides improvement when the mixed time scale is used in conjunction with the non-linear turbulence model, consistent with other thermal quantities. However, the opposite is true for the linear turbulence model, as shown in Figure. 20c.

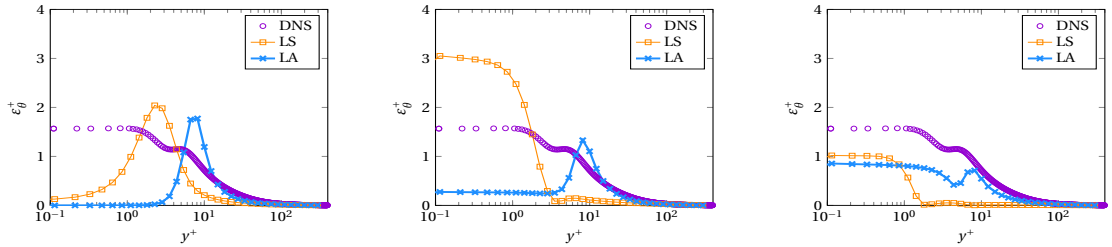

(a) *TV-R* (b) *TV-E* (c) *TV-M*

Figure 20: Dissipation of temperature variance obtained by *TV-R*, *TV-E* and *TV-M* for Pr= 10 at Re_τ= 395 with the explicit heat flux model

8 REFERENCES

[1] Kenichi Abe, Y. J. Jang, and Micheal A. Leschziner. An investigation of wall-anisotropy expressions and length-scale equations for non-linear eddy-viscosity models. *International Journal of Heat and Fluid Flow*, 24(2):181–198, 2003.

[2] E. Baglietto. An algebraic heat flux model in STAR-CCM+ for application to innovative reactors. `https://inis.iaea.org/search/search.aspx?orig{_}q=RN:47071158`, Toronto, 2011.

[3] Robert Bergant and Iztok Tiselj. Near-wall passive scalar transport at high Prandtl numbers. *Physics of Fluids*, 19(6), 2007.

[4] S. C. Chetal, V. Balasubramaniyan, P. Chellapandi, P. Mohanakrishnan, P. Puthiyavinayagam, C. P. Pillai, S. Raghupathy, T. K. Shanmugham, and C. Sivathanu Pillai. The design of the Prototype Fast Breeder Reactor. *Nuclear Engineering and Design*, 236(7-8):852–860, 2006.

[5] Bart J. Daly and Francis H. Harlow. Transport equations in turbulence. *Physics of Fluids*, 13(11):2634–2649, 1970.

[6] S. E. Elghobashi and B. E. Launder. Turbulent time scales and the dissipation rate of temperature variance in the thermal mixing layer. *Physics of Fluids*, 26(9):2415–2419, 1983.

[7] G. Grötzbach. Anisotropy and Buoyancy in Nuclear Turbulent Heat Transfer – Critical Assessment and Needs for Modelling. *Forschungszentrum Karlsruhe*, 2007.

[8] G. Grötzbach. Challenges in low-Prandtl number heat transfer simulation and modelling. *Nuclear Engineering and Design*, 264:41–55, 2013.

[9] K. Hanjalić. Modelling of Buoyancy Driven Turbulent Flows. *ERCOFTAC / IAHR Workshop on Refined Turbulence Modelling*, pages 1–27, 2008.

[10] K. Hanjalić and B. E. Launder. *Modelling Turbulence in Engineering and the Environment*. Cambridge University Press, 2011.

[11] N. Z. Ince and B. E. Launder. On the Computation of Buoyancy-Driven Turbulent Flows in Closed Cavities. *Int. J. Heat and Fluid Flow*, 10(TFD/87/9):110–117, 1987.

[12] Hiroshi Kawamura, Hiroyuki Abe, and K. Shingai. DNS of turbulence and heat transport in a channel flow with different Reynolds and Prandtl numbers and boundary conditions. *Turbulence Heat and Mass Transfer 3 (Proceedings of the Third Intl Symp. on Turbulence Heat and Mass Transfer)*, 1(July):15–32, 2000.

[13] Hiroshi Kawamura, Abe Hiroyuki, and Yuichi Matsuo. DNS of turbulent heat transfer in channel flow with respect to Reynolds and Prandtl number effects. *International Journal of Heat and Fluid Flow*, 20:196–207, 1999.

[14] Hiroshi Kawamura, Ohsaka Kouichi, Hiroyuki Abe, and Kiyoshi Yamamoto. DNS of turbulent heat transfer in channel flow with low to medium-high Prandtl number fluid. *International Journal of Heat and Fluid Flow*, 19:482–491, 1998.

[15] S. Kenjereš. *Numerical Modelling of Complex Buoyancy-Driven Flows*. University Delft, 1999.

[16] S. Kenjereš, S. B. Gunarjo, and K. Hanjalić. Contribution to elliptic relaxation modelling of turbulent natural and mixed convection. *International Journal of Heat and Fluid Flow*, 26(4 SPEC. ISS.):569–586, 2005.

[17] S. Kenjereš and K. Hanjalić. Prediction of turbulent thermal convection in concentric and eccentric horizontal annuli. *International Journal of Heat and Fluid Flow*, 16(5):429–439, 1995.

[18] S. Kenjereš and K. Hanjalić. Convective rolls and heat transfer in finite-length Rayleigh-Bénard convection: A two-dimensional numerical study. *Physical Review E - Statistical Physics, Plasmas, Fluids, and Related Interdisciplinary Topics*, 62(6):7987–7998, 2000.

[19] Ulrich Kleinhans, Christoph Wieland, Flemming J. Frandsen, and Hartmut Spliethoff. Ash formation and deposition in coal and biomass fired combustion systems: Progress and challenges in the field of ash particle sticking and rebound behavior. *Progress in Energy and Combustion Science*, 68:65–168, 2018.

[20] B. E. Launder. Heat and Mass Transport. *Topics in Applied Physics: Turbulence*, pages 231–287, 1976.

[21] B. E. Launder. On the Computation of Convective Heat Transfer in Complex Turbulent Flows. *Journal of Heat Transfer*, 110(4b):1112, 1988.

[22] B. E. Launder and B. I. Sharma. Application of the energy-dissipation model of turbulence to the calculation of flow near a spinning disc. *Letters in Heat and Mass Transfer*, 1(2):131–137, 1974.

[23] F. S. Lien, W. L. Chen, and M. A. Leschziner. Low-Reynolds-Number Eddy-Viscosity Modelling Based on Non-Linear Stress-Strain/Vorticity Relations. *Engineering Turbulence Modelling and Experiments*, pages 91–100, 1996.

[24] Sandro Manservisi and F. Menghini. A CFD four parameter heat transfer turbulence model for engineering applications in heavy liquid metals. *International Journal of Heat and Mass Transfer*, 69:312–326, 2013.

[25] Robert N. Meroney. An algebraic stress model for stratified turbulent shear flows, 1976.

[26] H. Müller, Bassam A. Younis, and B. Weigand. Development of a compact explicit algebraic model for the turbulent heat fluxes and its application in heated rotating flows. *International Journal of Heat and Mass Transfer*, 86:880–889, 2015.

[27] Y. Nagano. *Modelling Heat Transfer in Near-Wall Flows*. Cambridge University Press, 2010.

[28] OECD/NEA. Technology Roadmap Update for Generation IV Nuclear Energy Systems: Preparing Today for Tomorrow's Energy Needs, 2014.

[29] OpenFOAM. Block Mesh, 2020.

[30] I. Otić and G. Grötzbach. Turbulent heat flux and temperature variance dissipation rate in natural convection in lead-bismuth. *Nuclear Science and Engineering*, 155(3), 2007.

[31] I. Otić, G. Grötzbach, and M. Woerner. Analysis and modelling of the temperature variance equation in turbulent natural convection for low-Prandtl-number fluids. *Journal of Fluid Mechanics*, 525:237–261, 2004.

[32] D. M. Paes, P. R. Ribeiro, M. Shirdel, and K. Sepehrnoori. Study of asphaltene deposition in wellbores during turbulent flow. *Journal of Petroleum Science and Engineering*, 129:77–87, 2015.

[33] W Rodi. *The predictions of free turbulent boundary layers by use of a two-equation model of turbulence*. PhD thesis, University of London, 1972.

[34] F. Roelofs, A. Shams, I. Otic, M. Böttcher, M. Duponcheel, Y. Bartosiewicz, D. Lakehal, E. Baglietto, S. Lardeau, and X. Cheng. Status and perspective of turbulence heat transfer modelling for the industrial application of liquid metal flows. *Nuclear Engineering and Design*, 290(March 2011):99–106, 2015.

[35] Thomas Schulenberg and Robert Stieglitz. Flow measurement techniques in heavy liquid metals. *Nuclear Engineering and Design*, 240(9):2077–2087, 2010.

[36] Afaque Shams, F. Roelofs, E. Baglietto, S. Lardeau, and S. Kenjereš. Assessment and calibration of an algebraic turbulent heat flux model for low-Prandtl fluids. *International Journal of Heat and Mass Transfer*, 79:589–601, 2014.

[37] Ronald M. C. So and Charles G. Speziale. A Review of Turbulent Heat Transfer Modeling. *Annual Review of Heat Transfer*, 10(10):177–220, 1999.

[38] T. P. Sommer, R. M. C. So, and H. S. Zhang. Heat Transfer Modeling and the Assumption of Zero Wall Temperature Fluctuations. *Journal of Heat Transfer*, 116(4):855, 1994.

[39] unkown. Implementation Guide LienCubicKE. `https://personalpages.manchester.ac.uk/staff/david.d.apsley/turbmod.pdf`.

[40] Bassam A. Younis, Charles G. Speziale, and Timothy T. Clark. A rational model for the turbulent scalar fluxes. *Proceedings of the Royal Society A: Mathematical, Physical and Engineering Sciences*, 461(2054):575–594, 2005.

[41] Matthias Ziefuss, Nader Karimi, Florian Ries, Amsini Sadiki, and Amirfarhang Mehdizadeh. Entropy generation assessment for wall-bounded turbulent shear flows based on reynolds analogy assumptions. *Entropy*, 21(12):1–26, 2019.

[42] Matthias Ziefuss and Amirfarhang Mehdizadeh. A comprehensive assessment of the Reynolds Analogy in predicting heat transfer in turbulent wall-bounded shear flows. *International Journal of Heat and Fluid Flow*, 81(January):108527, 2020.